High Gamma Power Is Phase-Locked to Theta Oscillations in Human Neocortex

R. T. Canolty,[1*] E. Edwards,[1,2] S. S. Dalal,[3] M. Soltani,[1,2] S. S. Nagarajan,[3,4] H. E. Kirsch,[5] M. S. Berger,[6] N. M. Barbaro,[5,6] R. T. Knight[1,2,3,5,6]

We observed robust coupling between the high- and low-frequency bands of ongoing electrical activity in the human brain. In particular, the phase of the low-frequency theta (4 to 8 hertz) rhythm modulates power in the high gamma (80 to 150 hertz) band of the electrocorticogram, with stronger modulation occurring at higher theta amplitudes. Furthermore, different behavioral tasks evoke distinct patterns of theta/high gamma coupling across the cortex. The results indicate that transient coupling between low- and high-frequency brain rhythms coordinates activity in distributed cortical areas, providing a mechanism for effective communication during cognitive processing in humans.

Neuronal oscillations facilitate synaptic plasticity (*1*), influence reaction time (*2*), correlate with attention (*3*) and perceptual binding (*4*), and are proposed to play a role in transient, long-range coordination of distinct brain regions (*5*). Direct cortical recordings reveal that ongoing rhythms encompass a wide range of spatial and temporal scales—ultraslow rhythms less than 0.05 Hz coexist with fast transient oscillations 500 Hz or greater (*1*), with spatial coherence between these oscillations extending from several centimeters for the corticospinal tract (*6*) to the micrometer scale for subthreshold membrane oscillations in a single neuron (*7*). Exactly how these transient oscillations influence each other and coordinate processing at both the single-neuron and population levels remains unknown.

Evidence for cross-frequency coupling, where one frequency band modulates the activity of a different frequency band, is more abundant in animal than human data. For example, the theta rhythm can modulate the firing rate and spike timing of a single neuron (*8*–*11*) as well as the gamma power of the intracortical local field potential (*8*, *12*, *13*). Task-related changes in theta power have been observed in humans (*14*–*16*), and cross-frequency coupling at frequencies up to 40 Hz has been detected at the scalp (*17*, *18*). However, given the difficulty in localizing electrical sources from scalp recordings alone (*19*), subdural electrodes that record directly from the human cortex are needed to address this question. Furthermore, subdural electrodes are ideal for studying activity in the recently described human high gamma band (HG) at 80 to 150 Hz. HG activity is modulated by sensory, motor, and cognitive events (*20*), is functionally distinct from low gamma (30 to 80 Hz) with different physiological origins (*21*), and is correlated with the functional magnetic resonance imaging blood oxygen level–dependent (fMRI BOLD) signal (*22*–*24*). There have been no reports of coupling between any low-frequency rhythm and HG in signals recorded either at the scalp or directly from human sensory, motor, or association cortex. We therefore focus exclusively on theta/HG coupling in this report.

We analyzed multichannel subdural electrocorticogram (ECoG) data from five patients undergoing neurosurgical treatment for epilepsy. Typically, the events of interest in behavioral paradigms are the stimulus onsets and motor responses that evoke frequency-specific changes in the electrical activity of the brain. In contrast, the events of interest in cross-frequency coupling are features of the ongoing oscillatory activity itself. That is, cross-frequency coupling refers to statistical dependence between distinct frequency bands of the ongoing ECoG rather than dependence between the ECoG and external stimulus events. The dependence between two frequencies f_1 and f_2 can assume many forms, including coupling between the amplitude envelopes $A_1(t)$ and $A_2(t)$, the phase time series $\phi_1(t)$ and $\phi_2(t)$, or an amplitude-phase coupling between $A_1(t)$ and $\phi_2(t)$. We focus here on the last type of coupling and use an index of cross-frequency coupling that directly combines the amplitude envelope time series $A_1(t + \tau)$ of a high-frequency band with the phase time series $\phi_2(t)$ of a low-frequency band into one composite, complex-valued signal $z(t, \tau)$. The (normalized) temporal mean of this composite signal provides a sensitive measure of the coupling strength and preferred phase between the two frequencies (*25*).

Animal evidence for theta phase modulation of single-unit firing and the strong connection of theta to learning, attention, and memory (*26*, *27*) suggested to us that high-frequency oscillations in human neocortex may be modulated by the theta rhythm. Accordingly, we analyzed the ECoG across a range of behavior-

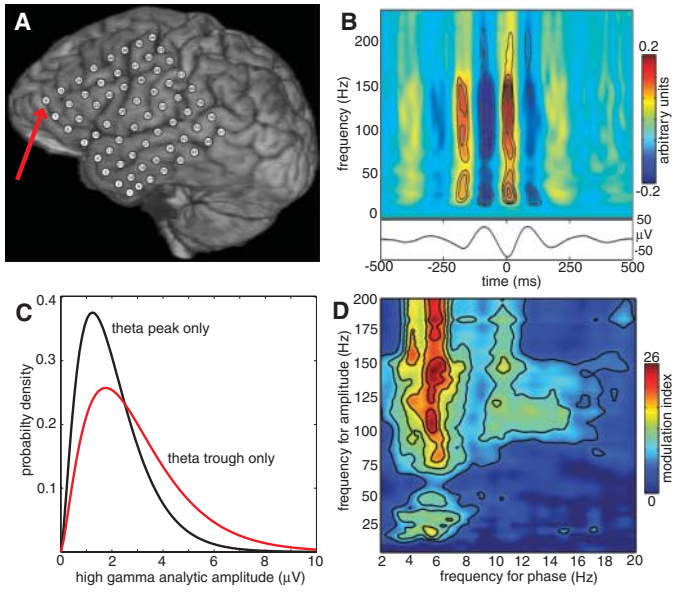

Fig. 1. High gamma (80 to 150 Hz) power is modulated by theta (4 to 8 Hz) phase. (**A**) Structural MRI showing position of 64-channel ECoG grid over frontal and temporal lobes in subject 1. (**B**) Example of phase-locked modulation of power in the ECoG signal from an electrode over the anterior portion of the middle frontal gyrus (arrow in Fig. 1A). (Top) Time-frequency plot of mean power modulation time-locked to the theta trough. Outermost contour indicates statistical significance ($P < 0.001$, corrected). Normalization permits comparison across frequencies; red and blue indicate a power increase or decrease, respectively, relative to the mean power. (Bottom) Theta trough–locked average of raw ECoG signal. (**C**) Best-fit gamma distributions for the high gamma analytic amplitude values that occurred at the peak (black, 0 radians) or the trough (red, π radians) of the theta waveform for the same electrode as in Fig. 1B. The difference in parameter values is significant ($P < 0.001$). (**D**) The modulation index (*25*) as a function of analytic amplitude (5 to 200 Hz) and analytic phase (2 to 20 Hz) for the same electrode as in Fig. 1B. Outermost contour indicates statistical significance ($P < 0.001$, corrected). Larger values indicate stronger cross-frequency coupling. Maximal coupling for this electrode is 146.2 Hz amplitude and 5.6 Hz phase (see also fig. S4).

[1]Helen Wills Neuroscience Institute, [2]Department of Psychology, University of California, Berkeley, CA 94720, USA. [3]Department of Bioengineering, [4]Department of Radiology, [5]Department of Neurology, [6]Department of Neurosurgery, University of California, San Francisco, CA 94143, USA.

*To whom correspondence should be addressed. E-mail: rcanolty@berkeley.edu

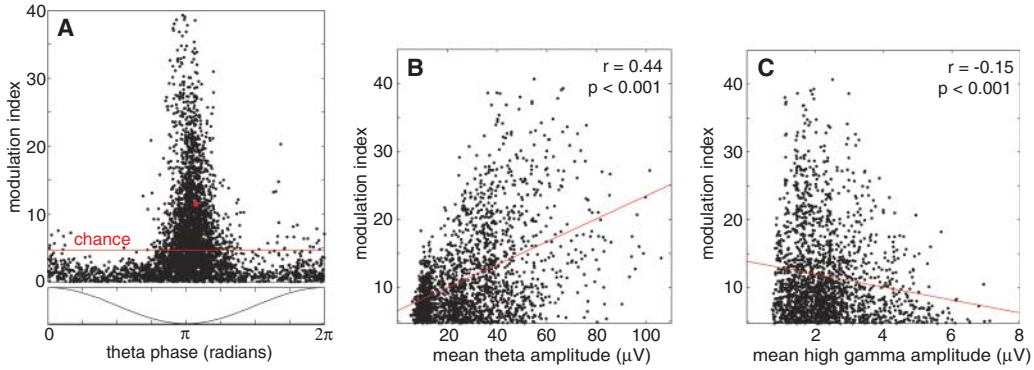

Fig. 2. Theta/HG coupling strength is a function of theta amplitude. (**A**) Theta/HG coupling strength and preferred theta phase. (Bottom) One theta cycle (schematic), from theta peak (0 radians) to trough (π radians) to peak (2π radians). (Top) Modulation index (*25*) computed separately for all electrodes in all subjects for each task. Larger magnitudes indicate stronger coupling (vertical axis), whereas the horizontal axis indicates the theta phase at which larger HG amplitudes tend to occur. Most electrodes with strong theta/HG coupling have a preferred theta phase of π, corresponding to the theta trough (see also Fig. 1C). The red dot indicates the electrode and recording block examined in Fig. 1. The red horizontal line corresponds to the significance threshold after correction for multiple comparisons. (**B**) Modulation index versus mean theta amplitude for all significant values from Fig. 2A (black dots) and best linear fit (red line), indicating their positive correlation. (**C**) Modulation index versus mean HG amplitude for all significant values from Fig. 2A (black dots) and best linear fit (red line), indicating their weak negative correlation (see also fig. S6).

al tasks (*25*). Figure 1B shows a time-frequency plot for data recorded from an electrode over the left middle frontal gyrus during an auditory language–related target detection task (Fig. 1A, arrow). Theta trough–locked averaging of the normalized time-frequency plane shows significant coupling ($P < 0.001$, corrected) between theta phase and high-frequency power, with an increase or decrease in power relative to baseline occurring at the theta trough or peak. Theta coupling was broadband from ~20 to 200 Hz, with the strongest modulation occurring in the HG band. Fig. 1D and fig. S4, using the modulation index discussed above, also show that coupling is strongest between theta phase and HG amplitude.

Across all tasks and subjects, 252 out of 299 tested electrodes (84.3%) showed significant theta/gamma coupling ($P < 0.001$ for each electrode, corrected). Excluding the 60 electrodes over resected tissue (which includes both epileptic and healthy tissue) increases this percentage to 88.7%, whereas only 66.7% of electrodes over resected tissue showed significant coupling. The largest HG amplitudes tended to occur at the trough of the theta waveform in electrodes with strong coupling (Figs. 1C and 2A). The coupling strength between the HG analytic amplitude time series $A_{HG}(t + \tau)$ and theta analytic phase $\phi_{TH}(t)$ should decrease to chance levels as the magnitude of the time lag τ increases. Figure 3A, displaying all ECoG electrodes for one subject, shows that this is indeed the case (see fig. S8 for all subjects).

The strength of theta/HG coupling depends on theta power as well as theta phase. We observed stronger coupling in electrodes with greater mean theta amplitude (Fig. 2B). That is, HG amplitudes have a stronger theta phase preference at greater theta power, indicating that theta/HG coupling strength can be modulated by adjusting theta power in a local cortical region. This contrasts with the weak negative correlation observed between theta/HG coupling strength and mean HG amplitude (Fig. 2C and fig. S6).

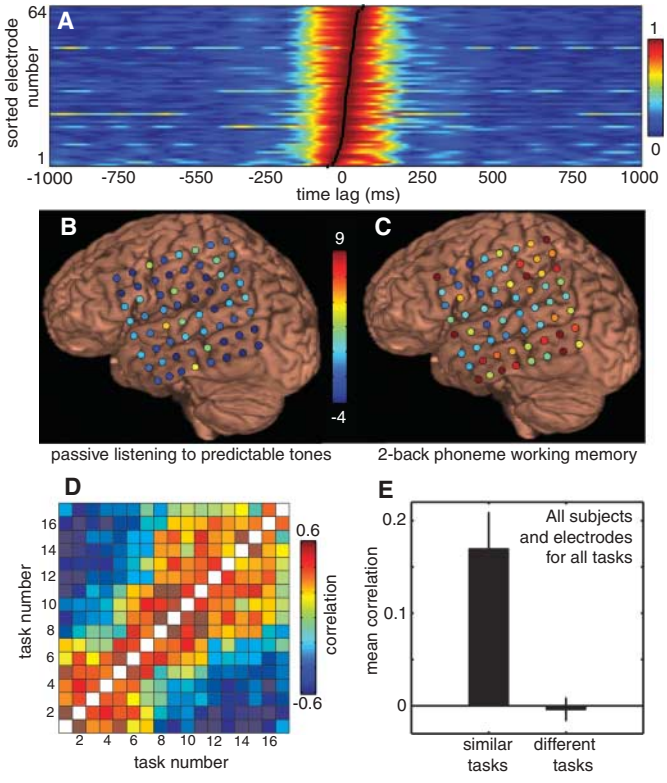

Fig. 3. Task-specific changes in the spatial pattern of theta/HG coupling strength. (**A**) Theta/HG coupling strength falls to chance at large time lags. Modulation index (*25*) as a function of lag for all electrodes over all tasks from subject 5. Electrodes are sorted by the time-lag τ_{max} associated with maximal coupling (black line). For ease of comparison, horizontal traces were renormalized so that the peak value for each channel is one (see also fig. S8). (**B**) The change in modulation index values from the mean for all electrodes in subject 2 during one task (passive listening to predictable tones). (**C**) As in (B), for a difficult working memory task. Subjects listened to a list of phonemes and responded when the current phoneme and the phoneme presented two items earlier were identical. (**D**) Similar tasks evoke similar spatial patterns of theta/HG coupling. Correlation matrix for all tasks in subject 2. Tasks: 1 to 4, passive listening to tones or phonemes; 5, mouth motor activation; 6, verb generation; 7, hand motor activation; 8 to 11 auditory working memory; 12 and 13, linguistic target detection; 14 to 17, auditory-vibrotactile target detection (see SOM text). (**E**) Mean correlation and standard error between similar tasks (positive, $P < 0.01$, corrected, 58 task pairs) as well as different tasks (not significant, 617 task pairs) for all electrodes in all subjects over all tasks.

Thus, mean HG power and the strength of theta/HG coupling appear to reflect independent dimensions of cortical activity.

Task-dependent modulation of theta power has been shown in humans (*26*), prompting the hypothesis that theta/HG coupling may be task-dependent. Two examples of task-specific changes in the spatial pattern of theta/HG coupling strength over all electrodes in one subject are shown in Fig. 3, B and C. Figure 3D shows that behavioral tasks evoke distinct and reproducible patterns of coupling in this subject, with similar tasks evoking similar coupling patterns whereas different tasks evoked alternate patterns. Spatial patterns associated with two runs of similar tasks were positively correlated, whereas runs

of different tasks exhibited a null or negative correlation. This trend held across all tasks and subjects, as shown by Fig. 3E. These results are consistent with the hypothesis that transient cross-frequency coupling modulates network engagement, enabling flexible control of cognitive processing.

Oscillations are rhythmic fluctuations in neuronal excitability that modulate both output spike timing and sensitivity to synaptic input (*5*). Therefore, effective communication between neuronal populations requires precise matching of the relative phase of distinct rhythms to axonal conduction delays. An oscillatory hierarchy operating across multiple spatial and temporal scales could regulate this proposed long-range communication (*13*). Basal forebrain cortical-projecting GABAergic (γ-aminobutyric acid–releasing) neurons are well positioned to control theta/HG coupling; these neurons preferentially synapse onto intracortical GABAergic neurons throughout the cortex, with disinhibitory spike bursts causing a brief increase in gamma power at the theta trough (*28*). Our observations that (i) HG power is modulated by theta phase, (ii) an increase in theta power strengthens theta/HG coupling, and (iii) the topography of theta/HG coupling is task-dependent support the hypothesis that cross-frequency coupling between distinct brain rhythms facilitates the transient coordination of cortical areas required for adaptive behavior in humans.

References and Notes

1. G. Buzsaki, A. Draguhn, *Science* **304**, 1926 (2004).
2. K. Linkenkaer-Hansen, V. V. Nikulin, S. Palva, R. J. Ilmoniemi, J. M. Palva, *J. Neurosci.* **24**, 10186 (2004).
3. T. Womelsdorf, P. Fries, P. P. Mitra, R. Desimone, *Nature* **439**, 733 (2006).
4. J. P. Lachaux *et al.*, *Neuroimage* **25**, 491 (2005).
5. P. Fries, *Trends Cogn. Sci.* **9**, 474 (2005).
6. J. M. Schoffelen, R. Oostenveld, P. Fries, *Science* **308**, 111 (2005).
7. E. M. Izhikevich, *Neural Netw.* **14**, 883 (2001).
8. A. Bragin *et al.*, *J. Neurosci.* **15**, 47 (1995).
9. G. Buzsaki *et al.*, *Neuroscience* **116**, 201 (2003).
10. A. G. Siapas, E. V. Lubenov, M. A. Wilson, *Neuron* **46**, 141 (2005).
11. H. Lee, G. V. Simpson, N. K. Logothetis, G. Rainer, *Neuron* **45**, 147 (2005).
12. J. J. Chrobak, G. Buzsaki, *J. Neurosci.* **18**, 388 (1998).
13. P. Lakatos *et al.*, *J. Neurophysiol.* **94**, 1904 (2005).
14. A. D. Ekstrom *et al.*, *Hippocampus* **15**, 881 (2005).
15. P. B. Sederberg, M. J. Kahana, M. W. Howard, E. J. Donner, J. R. Madsen, *J. Neurosci.* **23**, 10809 (2003).
16. J. Onton, A. Delorme, S. Makeig, *Neuroimage* **27**, 341 (2005).
17. B. Schack, N. Vath, H. Petsche, H. G. Geissler, E. Moller, *Int. J. Psychophysiol.* **44**, 143 (2002).
18. J. M. Palva, S. Palva, K. Kaila, *J. Neurosci.* **25**, 3962 (2005).
19. P. L. Nunez, R. S. Srinivasan, *Electric Fields of the Brain: The Neurophysics of EEG* (Oxford Univ. Press, Oxford, 2005).
20. N. E. Crone, D. L. Miglioretti, B. Gordon, R. P. Lesser, *Brain* **121**, 2301 (1998).
21. E. Edwards, M. Soltani, L. Y. Deouell, M. S. Berger, R. T. Knight, *J. Neurophysiol.* **94**, 4269 (2005).
22. N. K. Logothetis, J. Pauls, M. Augath, T. Trinath, A. Oeltermann, *Nature* **412**, 150 (2001).
23. R. Mukamel *et al.*, *Science* **309**, 951 (2005).
24. J. Niessing *et al.*, *Science* **309**, 948 (2005).
25. Materials and methods are available as supporting material on *Science* Online.
26. M. J. Kahana, D. Seelig, J. R. Madsen, *Curr. Opin. Neurobiol.* **11**, 739 (2001).
27. R. Miller, *Cortico-Hippocampal Interplay and the Representation of Contexts in the Brain* (Springer-Verlag, New York, 1991).
28. S. C. Lin, D. Gervasoni, M. A. L. Nicolelis, *J. Neurophysiol.* (2006); doi: 10.1152/jn.00524.2006.

29. This work was supported by the Rauch family, National Institute of Neurological Disorders and Stroke grant NS21135, NSF Fellowship 2004016118, and National Institute on Deafness and Other Communication Disorders grant F31DC006762. The authors thank P. Garcia and D. Filippi of the Department of Neurology, University of California San Francisco, for their help on electrical stimulation mapping and localizing epileptic tissue.

Supporting Online Material

www.sciencemag.org/cgi/content/full/313/5793/1626/DC1
Materials and Methods
SOM Text
Figs. S1 to S8

30 March 2006; accepted 20 July 2006
10.1126/science.1128115

Caveolin-1 Is Essential for Liver Regeneration

Manuel A. Fernández,[1,2]* Cecilia Albor,[1]* Mercedes Ingelmo-Torres,[1] Susan J. Nixon,[2] Charles Ferguson,[2] Teymuras Kurzchalia,[3] Francesc Tebar,[1] Carlos Enrich,[1] Robert G. Parton,[2]† Albert Pol[1]†

Liver regeneration is an orchestrated cellular response that coordinates cell activation, lipid metabolism, and cell division. We found that *caveolin-1* gene–disrupted mice (*cav1*$^{-/-}$ mice) exhibited impaired liver regeneration and low survival after a partial hepatectomy. Hepatocytes showed dramatically reduced lipid droplet accumulation and did not advance through the cell division cycle. Treatment of *cav1*$^{-/-}$ mice with glucose (which is a predominant energy substrate when compared to lipids) drastically increased survival and reestablished progression of the cell cycle. Thus, caveolin-1 plays a crucial role in the mechanisms that coordinate lipid metabolism with the proliferative response occurring in the liver after cellular injury.

The liver is pivotally positioned in the regulation of the body's metabolic homeostasis of lipids, carbohydrates, and vitamins. In addition, it produces essential serum proteins, lipoproteins, enzymes, and cofactors. Paradoxically, the liver is also the main detoxifying organ in the body, being continuously exposed to the threat of cellular injury. Consequently, the liver has evolved complex regenerative mechanisms to respond to chemical, traumatic, or infectious injuries (*1*–*3*). During regeneration, the liver continues to accomplish its critical functions, such as glucose homeostasis, protein synthesis, and bile secretion. Liver regeneration does not require stem cells but instead occurs when differentiated and largely quiescent hepatic cells reenter the cell cycle to replace the lost functional mass.

One of the most extensively characterized model systems to study liver regeneration is the partial hepatectomy in rodents. In this model, the left and medial lobes of the liver are excised, resulting in removal of 70% of the hepatic mass. Within minutes, hepatocytes then undergo a coordinated cellular activation termed the acute phase response. This highly regulated process is simultaneously mediated by different growth factors and cytokines that conduct the response signal into kinases and transcription factors. As a result of the acute response, the hepatocyte initiates the transcription of more than 100 early genes, accumulates triacylglycerol and cholesterol esters in intracellular lipid droplets (*4*), and progresses through the cell cycle. Lipid droplet formation is an essential part of the proliferative response during liver regeneration (*5*). Lipids stored in lipid droplets are delivered into the bile or used in the production of new lipoproteins and bile acids, for the synthesis of new membranes, or to supply the energy required for remnant hepatocytes to rebuild the liver. By compensatory hyperplasia, the regenerative process reestablishes the original liver mass in approximately 1 week, after which hepatocytes return to a quiescent state.

Caveolae are distinct domains of the plasma membrane of most cells, where cellular processes such as signaling and membrane sorting occur in a highly regulated lipid and protein environment (*6*). Caveolin, an essential component of caveolae, is a protein that has the distinct capability to create these highly ordered domains at the cell surface. In addition, caveolin and caveolae are key elements in the regulation of the intracellular homeostasis of lipids, cell activation, and cell

[1]Departament de Biologia Cellular, Facultat de Medicina, Institut d'Investigacions Biomèdiques August Pi i Sunyer, Universitat de Barcelona, Casanova 143, 08036 Barcelona, Spain. [2]Institute for Molecular Bioscience, Centre for Microscopy and Microanalysis and School of Biomedical Sciences, University of Queensland, Brisbane, Queensland 4072, Australia. [3]Max-Plank-Institute of Molecular Cell Biology and Genetics, Pfotenhauerstrasse 108, 01307 Dresden, Germany.

*These authors contributed equally to this work.
†To whom correspondence should be addressed. E-mail: R.Parton@imb.uq.edu.au (R.G.P.); apols@ub.edu (A.P.).